



Contents lists available at ScienceDirect

Powder Technology

journal homepage: www.elsevier.com/locate/powtec

Powder metallurgical processing of Co–28%Cr–6%Mo for dental implants: Physical, mechanical and electrochemical properties

Wilson Corrêa Rodrigues, Luiz Roberto Broilo, Lírio Schaeffer, Gerhard Knörnschild*, Fidel Romel Mallqui Espinoza

Department of Metallurgy, Federal University of Rio Grande do Sul, Porto Alegre, Brazil

ARTICLE INFO

Article history:

Received 22 October 2009
Received in revised form 8 July 2010
Accepted 17 September 2010
Available online xxxx

Keywords:

Dental implants
Cobalt alloys
Powder metallurgy
Sintering

ABSTRACT

The parameters for conventional powder-metallurgical production of a CoCrMo alloy for dental implants were determined. With the application of these parameters an alloy with sufficient green density, low porosity after sintering, considerable hardness and spontaneously passive behavior in the Ringer solution can be achieved. The comparison of samples with different sintering temperatures revealed that a slight variation of the sintering temperature can have a considerable effect on the physical, mechanical and electrochemical properties of the alloy.

© 2010 Elsevier B.V. All rights reserved.

1. Introduction

CoCrMo alloys are widely used in total hip and knee replacements, dental devices and support structures for heart valves [1]. They are the preferred alloys for articular applications with metal-on-metal contact [2,3] since the tribological properties are superior in comparison with those of titanium alloys.

Biocompatibility of cobalt alloys is based on the spontaneous formation of a passivating oxide film. Disruption by mechanical loading of this very thin film [4] leads to metal ion release. Problems with the release of metal ions from corroding implant material were reported by various authors [5–7]. In the case of CoCrMo dental alloys the leaching of the Co, Cr, Fe, Zn and Ni ions in the solution was measured by Rincic [8].

While titanium alloys have an extended passive range, CoCrMo alloys show a transition to transpassive behavior at moderate electrode potentials. The transpassive behavior is described as an accelerated uniform dissolution through the passive film [9] or as a localized breakdown of passivity, caused by mechanical events such as fretting corrosion [10] or by microstructural characteristics such as sensitization [11]. Vidal et al. [12] showed in his work that the corrosion rate depends on the microstructure produced by different heat treatments. Wear resistance, mechanical properties, biocompatibility and corrosion resistance may be influenced by the microstructure which depends on the thermal treatment applied to the material.

The microstructure is also strongly influenced by the manufacturing process of the implant. Early comparative studies of cast vs. wrought alloys stated a better corrosion resistance of the wrought alloys [13,14]. The finer grain size and more uniform/finer distribution of the carbides in the wrought alloy contribute to its chemical homogeneity and improved corrosion behavior, according to [14,15]. In the case of wrought CoCrMo alloys, fabricated by hot-forging, Lee et al. [16] found a strong influence of the carbon content on the microstructure and mechanical properties. Rodriguez et al. [17] reported that a lower carbon content in the CoCrMo alloys could contribute to greater chemical and microstructural homogeneity and thus a better corrosion resistance.

Until now, less attention has been paid to powder-metallurgical (P/M) fabrication techniques. Some researchers studied the microstructure and mechanical properties of (P/M)-CoCrMo alloys. Song et al. [18] studied carbide precipitation at grain boundaries and in the bulk of CoCrMo compacted powders as a function of the sintering temperature between 900 °C to 1100 °C. They observed that at temperatures above 1100 °C, no carbide precipitation occurred indicating that carbides were not stable at these temperatures. The same authors [19] examined the formation of athermal epsilon-martensite in (P/M)-CoCrMo alloy after rapid cooling from sintering temperature. They found that the amounts of epsilon-martensite were 3–4-fold those found in conventional alloys, suggesting that the powder structure provides increasing nucleation sites for athermal epsilon-martensite.

Okșiuta [20] produced a (P/M)-CoCrMo alloy for bio-implants by green compact sintering, rotary cold repressing and heat treatment. They observed that rotary cold repressing favors the formation of the

* Corresponding author.

E-mail address: gerhard.hans@ufrgs.br (G. Knörnschild).

HCP-phase. By an appropriate heat treatment a homogeneous alpha-Co structure, with good ductility could be obtained.

Sato et al. [21] chose hot pressing in N₂-containing atmosphere as a production way for (P/M)-CoCrMo alloys. The results showed that the microstructure, including the formation of the Cr₂N-phase, as well as the mechanical properties are a function of the N₂-content, pressure and temperature of the atmosphere during hot pressing.

Powder-metallurgical (P/M) techniques enable the production of materials with special properties, which cannot be obtained by many other methods. Recently implant materials with a dense core and a porous outer layer to promote tissue growth for better implant fixation were produced [22,23]. Frequently hot isostatic pressing is applied as a post-sintering step within these complex production procedures [12,24].

Dabrowski et al. [25] used (P/M) CoCrMo for the production of composite materials. They approved the following additives for further research: calcium pyrophosphate, boron carbide and silicon nitride.

Other fabrication processes, like combustion synthesis [1] have also been tried in the last years. Tandon [26] developed metal injection molding as a new production way for biomedical CrCrMo-alloys.

Apart from high-cost, complex (P/M)-production ways to produce superior materials like porosity graded alloys, it is also of interest to search for simpler (P/M)-methods in order reduce costs and to develop near net shape techniques which might become more competitive with methods like forging or casting.

Therefore, the application of a rather simple, conventional powder-metallurgical way for the production of a dental Co–28%Cr–6%Mo alloy was studied in the present work. Powder processing, sintering, and the influence of sintering temperature on the mechanical properties and on the electrochemical behavior in the Ringer solution were tested.

2. Experimental procedure

The raw material was a CoCrMo alloy powder with the composition presented in Table 1. The powder, delivered by Powder Alloy Corporation, was produced by water atomization. The alloy powder particles have a spherical shape (Fig. 1) and the granulometry, according to the manufacturer, is the following: +325 mesh: 10%, –325 mesh: 90%. Zinc stearate (3 wt.%) was added as a lubricant and mixed during 2 h in a V-cone type mixer at 24 rpm. This additive appears in the micrograph (Fig. 1) as a non-spherical “impurity”.

The compactibility curve of the powder mixtures was determined according to ASTM B331, using a 40 ton hydraulic press (Eka) with double action die compaction. Compacting pressures varying from 200 MPa to 1000 MPa were applied to produce cylindrical samples of 12 mm diameter and 4 mm height. From the compactibility curve (Fig. 2) 800 MPa was considered the optimum compacting pressure, since the green density of 6.12 g/cm³, reached at 800 MPa, could not be improved by applying a higher pressure.

Sintering was performed in a tube furnace in an atmosphere of 75 vol% N₂/25 vol% H₂, at temperatures of 1150 °C, 1280 °C and 1300 °C, respectively.

The sintering procedure consisted of:

1. Heating up to 480 °C, at a rate of 10 °C/min.
2. Constant temperature T = 480 °C during 120 min. Burning of the lubricant happens during this stage of the treatment.

Table 1
Chemical composition of the CoCrMo alloy powder.

Element	Co	C	Cr	Mo	Ni	Mn	Si	Fe
Weight %	Balance	0.35	28.5	6.0	1.0	1.0	1.0	0.75

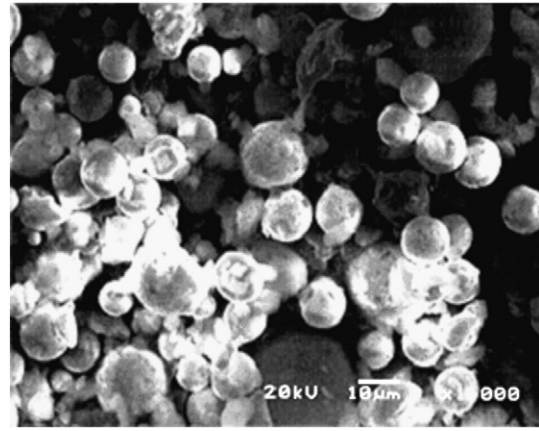


Fig. 1. Co–28%Cr–6%Mo powder with zinc stearate.

3. Further heating at 10 °C/min up to a sintering temperature of 1150 °C, 1280 °C or 1300 °C, respectively.
4. Sintering at a constant temperature during 60 min.
5. Cooling at a medium rate of 20 °C/min.

The microstructure of the sintered specimens was analyzed by optical and scanning electron microscopy and by statistical image analysis. For the calculation of the grain size the diameter of a circle with an equivalent area to a grain was taken as the size of the grain. The same procedure was used to determine the average size of the carbides.

Electrochemical tests were performed in a standard three-electrode glass cell using a potentiostat Intelligence Control Bank LB95 with an interface for computer controlled data acquisition. The cylindrical samples were ground with grade 2000 emery paper and a copper wire was fixed at the back side for electrical contact. The wire was isolated by a glass tube; back side and lateral sides of the samples were isolated by epoxy resin. The front side, exposed to the electrolyte, had an area of 1.13 cm². Potentiodynamic tests were performed in the Ringer solution (9 g/L NaCl, 0.17 g/L CaCl₂·2H₂O, 0.4 g/L KCl, 2.1 g/L NaHCO₃). The solution was kept at 37 °C by a thermostat. Voltage scans were started at a potential of –100 mV vs. normal hydrogen electrode (NHE). The scan direction was inverted when the anodic current density surpassed 10 mA/cm². The scan rate was 0.4 mV/s. After the tests the samples were examined by scanning electron microscopy.

3. Results and discussion

3.1. Physical properties

Fig. 3a, b and c represent the sintered, polished samples without chemical attack to reveal the grade of porosity as a function of the sintering temperature. The density of the samples after sintering was measured applying Archimedes' principle according to MPIF-95 norm.

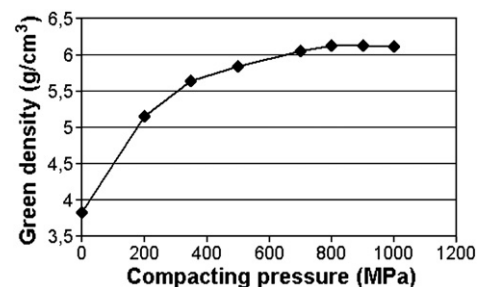


Fig. 2. Compressibility curve of the Co–28%Cr–6%Mo powder.

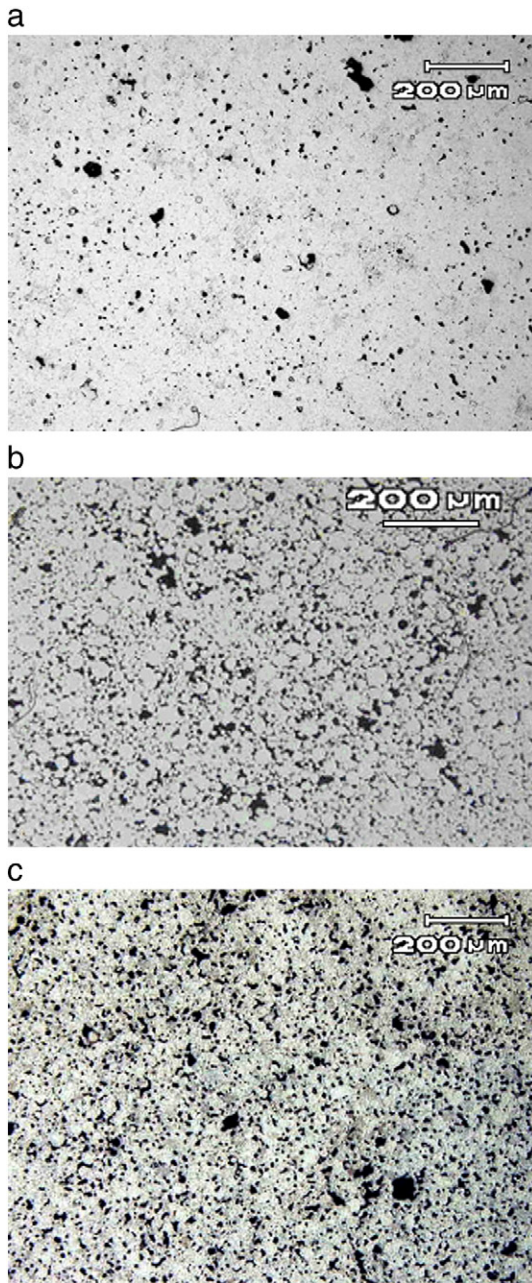


Fig. 3. Samples after sintering; polished surface; sintering temperature: a) 1300 °C; b) 1280 °C; and c) 1150 °C.

At 1150 °C, only 75.2% of the theoretical density, according to ASTM F75-98 [27], was achieved, while at 1280 °C and 1300 °C, 91.6% and 94.2%, respectively, of the theoretical value of 8.34 g/cm³ were measured (Fig. 4). Measurements with five samples showed that

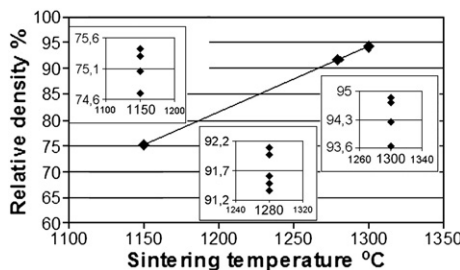


Fig. 4. Relative density as a function of the sintering temperature.

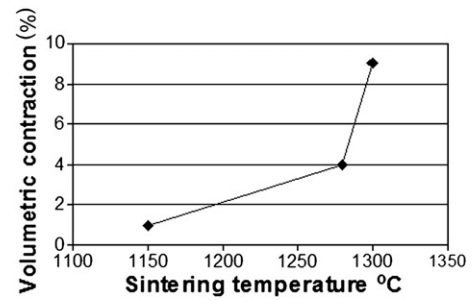


Fig. 5. Volumetric contraction as a function of the sintering temperature.

these values are reproducible within $\pm 0.7\%$ (see inserts in Fig. 4). The corresponding values of volumetric contraction during the sintering heat treatment are shown in Fig. 5.

3.2. Mechanical properties and microstructure

The microstructure of the alloy consists of a cobalt matrix with chromium and molybdenum carbides at the grain boundaries and within the grains (Fig. 6). The matrix grains of the CoCrMo (1300 °C) samples are coarser than that of CoCrMo(1280 °C), as the image analyses (Table 2) showed: An average grain size of 8.2 μm was calculated for CoCrMo(1280 °C) and of 12.5 μm for CoCrMo(1300 °C). Analysis of the grain size distribution (Fig. 7) reveals that in the CoCrMo (1300 °C) samples bigger grains ($d > 25 \mu\text{m}$) are statistically overrepresented, obviously as the result of the isolated growth of a part of the grains at that temperature. Matrix carbides are smaller in the CoCrMo (1300 °C) samples (Table 2). Matrix carbides are of globular shape in CoCrMo(1280 °C) as well as in the CoCrMo(1300 °C) samples. Grain boundary carbides are about 50% bigger in the CoCrMo(1300 °C) samples, and the size distribution is less uniform than in the case of

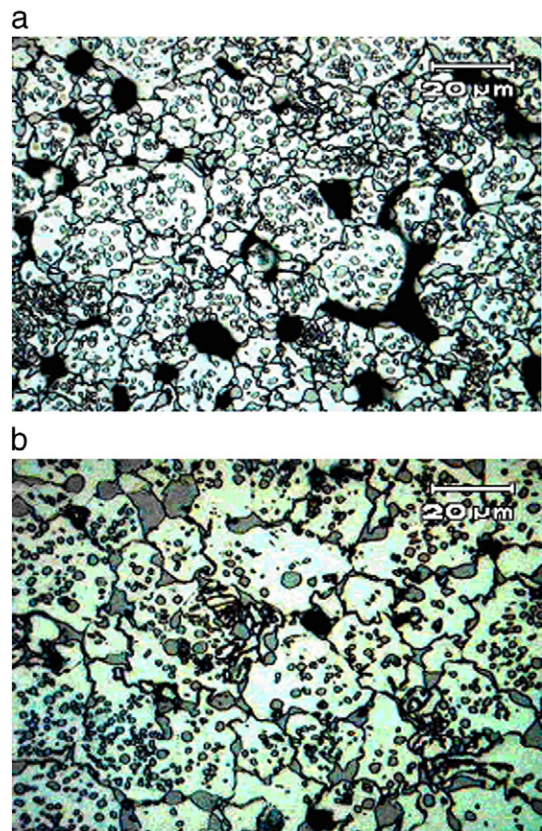
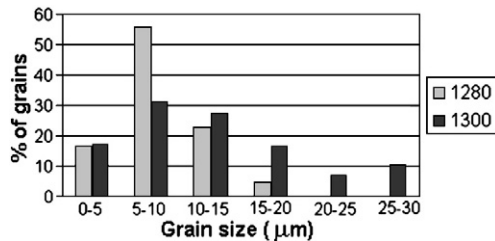


Fig. 6. Microstructure of sintered samples (Etchant: Marble's reagent). Sintering temperature: a) 1280 °C; b) 1300 °C.

Table 2
Microstructure analysis of sintered materials.

	Average grain size (μm)	Matrix carbides (μm)	Grain boundary carbides (μm)	Carbide volume (%)	Fraction of g.b. covered by carbides (%)
1280 °C	8.2	2.2	2.1	39	53
Standard deviation	3.54	0.65	0.77		
1300 °C	12.5	1.6	2.9	32	43
Standard deviation	64.24	0.55	1.60		

**Fig. 7.** Grain size distribution of sample sintered at 1280 °C and 1300 °C, respectively.

CoCrMo(1280 °C). There is a tendency to the formation of bigger carbides at grain boundary triple points. Grain boundary carbides in the CoCrMo(1280 °C) samples are elongated in the direction of the grain boundary. The volume fraction of carbides is 39% in the 1280 °C sample and 32% in the 1300 °C sample. In both, CoCrMo(1280 °C) and CoCrMo(1300 °C), grain boundaries are partially covered by carbides. From the microstructural characteristics of the CoCrMo(1300 °C) samples, outlined above, bigger matrix grains, coarser grain boundary carbides and lower volume fraction of carbides, a lower coverage with carbides of the grain boundaries in CoCrMo(1300 °C) can be expected. This was confirmed by quantitative image analysis: In the CoCrMo(1280 °C) samples 53% of the grain boundaries are covered by carbide, but only 43% in the case of CoCrMo(1300 °C). The results of the microstructure analysis are summarized in Table 2.

According to Levine [28], the discontinuous carbide formation along the grain boundaries, as observed in the 1280 °C and the 1300 °C samples, is a desirable condition for strength and ductility in F75 alloys, while massive, continuous grain boundary carbides as well as completely clean grain boundaries without carbides lead to a reduction of ductility or of strength, respectively.

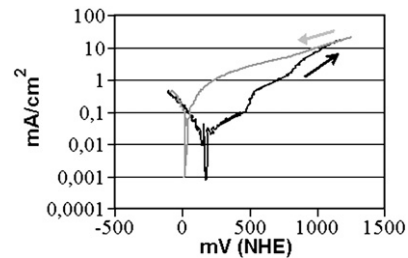
Despite of the bigger grain size and the lower carbide fraction the CoCrMo(1300 °C) samples reached a higher micro-hardness (Table 3). Also, a lower carbide coverage of the grain boundaries in comparison with CoCrMo(1280 °C) should rather diminish micro-hardness, according to [28]. Therefore, it can be assumed that the principal reason of the higher micro-hardness is the lower porosity of the CoCrMo(1300 °C) samples.

3.3. Electrochemical properties

The voltammograms of the samples with the three different sintering temperatures showed that the CoCrMo alloy is spontaneously passivated in the test solution. The curves begin with a cathodic

Table 3
Micro-hardness and density of Co–28%Cr–6%Mo as a function of the sintering temperature.

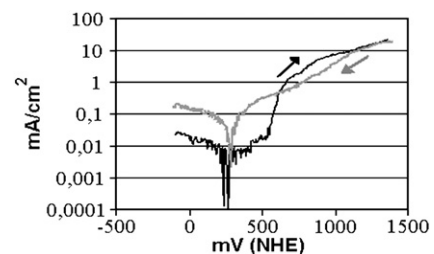
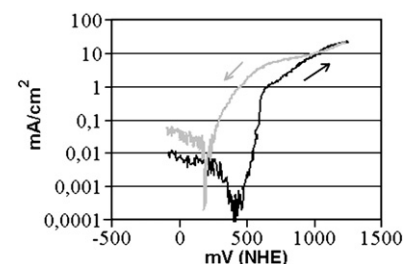
Sintering temperature (°C)	Sintered density (g/cm^3)	Micro-hardness (Hv_{30})
1300	7.86	434
1280	7.64	349
1150	6.27	258

**Fig. 8.** Potentiodynamic test with Co–28Cr–6Mo, sintered at 1150 °C; Ringer solution, 37 °C, $dU/dt = 0.4$ mV/s.

current, followed by a passive range with a low anodic current density. No active–passive transition was observed in all three cases (Figs. 8–10). The comparison of the voltammograms with those of pure Co, Cr and Mo, published by Kocijan et al. [29] shows that the electrochemical behavior of the CoCrMo alloy at higher potentials is strongly influenced by Cr. The samples remained passive up to the sudden current rise by the transpassive oxidation of Cr(III) to Cr(VI). The breakthrough potential for transpassive oxidation (defined in this work as the potential where the current density surpasses $0.1 \text{ mA}/\text{cm}^2$), measured during the scan in the anodic direction (Figs. 8–10), increases with the sintering temperature from +455 mV (NHE) for CoCrMo(1150 °C), to +575 mV for CoCrMo(1280 °C) and +590 mV(NHE) for CoCrMo(1300 °C).

The reverse scan in the cathodic direction reveals the capacity of the alloy to reestablish the passive state. The repassivation potential (defined in this work as the potential where the current density falls below $0.1 \text{ mA}/\text{cm}^2$) was reached by the CoCrMo(1150 °C) sample only at +60 mV(NHE), at +345 mV(NHE) by CoCrMo(1280 °C) and at +293 mV(NHE) by CoCrMo(1300 °C). This means, that between transpassive breakdown and repassivation potential a hysteresis is observed, which is about 400 mV for CoCrMo(1150 °C), 230 mV for CoCrMo(1280 °C), and 300 mV for CoCrMo(1300 °C), indicating the best repassivation behavior for CoCrMo(1280 °C).

Differences are also evident in the open circuit potential, established during 1 h of measurement (Fig. 11). The alloys sintered at 1280 °C and at 1300 °C have both a similar open circuit potential of

**Fig. 9.** Potentiodynamic test with Co–28Cr–6Mo, sintered at 1280 °C; Ringer solution, 37 °C, $dU/dt = 0.4$ mV/s.**Fig. 10.** Potentiodynamic test with Co–28Cr–6Mo, sintered at 1300 °C; Ringer solution, 37 °C, $dU/dt = 0.4$ mV/s.

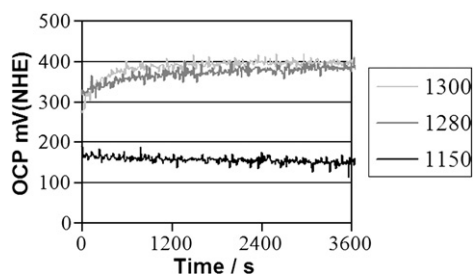


Fig. 11. Open circuit potentials of Co–28Cr–6Mo, sintered at 1150 °C, 1280 °C e 1300 °C, respectively. Ringer solution, 37 °C.

about +400 mV(NHE), which is about 250 mV nobler than that of CoCrMo(1150 °C). The open circuit potentials are in accordance with the corrosion potential in the potentiodynamic curves, indicating that the samples are passive from the beginning of the test. It is remarkable that open circuit and corrosion potentials in this work are considerably nobler than the values reported in the literature for cast and wrought CoCrMo alloys under similar conditions [29], while the potentials for transpassive breakthrough are similar to literature data. The shift of the corrosion potential can be caused by a lower anodic current or by a higher cathodic current. The higher corrosion potential might be a consequence of the high carbide concentration of the samples examined in the present work. Carbides represent cathodic sites, thus the higher carbide portion elevates the cathodic current. Vidal et al. [12] found that the properties of the passive film on CoCrMo depend of the thermal treatment, with a higher passive current for alloys with a higher carbide content. However, this effect does not seem to be significant in the present work, since it would make the corrosion potential more negative. Obviously a higher cathodic current and an approximately constant anodic current shift the corrosion potential to higher values.

The electrochemical behavior of CoCrMo(1150 °C) is determined by the relatively low density of only 75% of the theoretical value. The low volumetric contraction of only about 1% (Fig. 5) demonstrates that the sintering process is obviously slow at this temperature.

Scanning electron microscopic (SEM) examinations showed the accumulation of corrosion products at the pores of the CoCrMo (1150 °C) alloy, indicating these defects as the preferred points of localized corrosion attack (Fig. 12). The high porosity is also the most probable reason for the higher current density in the passive region of this alloy. All three alloys are covered by a thick film after the potentiodynamic tests due to the fact that they were polarized up to the transpassive potential region (Figs. 13, 14). The transpassive attack at the CoCrMo(1280 °C) sample is uniform, but with accelerated dissolution of the matrix close to the matrix/carbide interfaces (Fig. 13). The film is interrupted at grain boundaries and matrix/grain-boundary–carbide interfaces (Fig. 14). The morphology of the CoCrMo

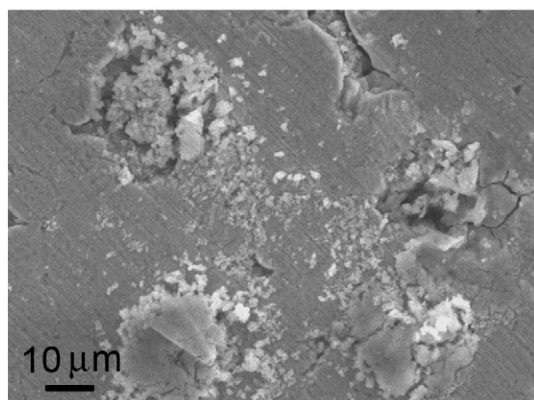


Fig. 12. CoCrMo(1150 °C) alloy: Corrosion products after potentiodynamic test (SEM).

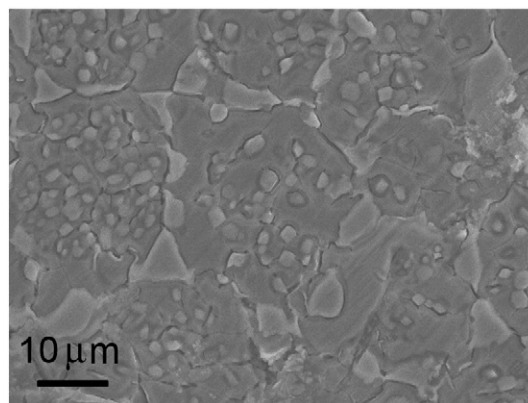


Fig. 13. Surface of CoCrMo(1280 °C) after potentiodynamic test (SEM).

(1300 °C) samples was very similar, however, these samples showed first signs of softening during the sintering treatment, impairing the dimensional stability of the sample. This agrees with information about incipient melting during the formation of porous coatings which were applied at temperatures around 1300 °C in order to achieve strong particle–particle and particle–substrate bonds [30]. The different mechanisms of transpassive dissolution, localized attack in the CoCrMo(1150 °C) alloy and uniform dissolution in the CoCrMo (1280 °C) and the CoCrMo(1300 °C) alloy, are responsible for the different breakthrough potentials. The localized attack in the CoCrMo (1150 °C) alloy begins about 120 mV below the transpassive dissolution of the other two alloys. The small difference between the breakthrough potentials of CoCrMo(1280 °C) and CoCrMo (1300 °C) might be due to a different chromium content in the matrix or close to the matrix/carbide interfaces. With less carbides the chromium content in the CoCrMo(1300 °C) matrix should be slightly higher. This explains the slightly higher breakthrough potential, supposed that the chromium influence is the same as that observed in the transpassive breakthrough of ferrous alloys [31,32].

4. Conclusions

The study has shown that conventional powder metallurgy is a promising way to obtain a CoCrMo alloy for dental implant applications by a cost-reducing procedure. With the parameters found for compaction and heat treatment the resultant alloy is characterized by a sufficient green density, a density after sintering of 92% of the theoretical value and passive electrochemical behavior in the Ringer solution. The sintering temperature was the parameter with the strongest influence on microstructure, mechanical and electrochemical properties. From the three sintering temperatures tested, 1150 °C was found to give poor results for the density of

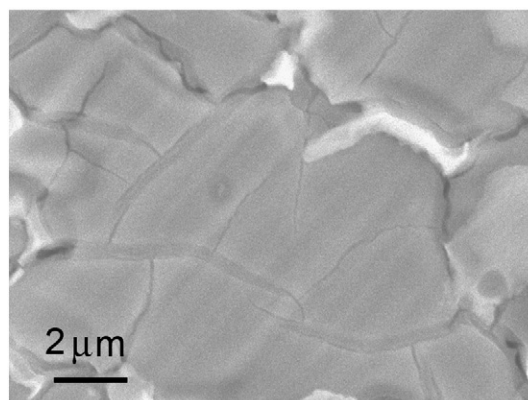


Fig. 14. Film on the CoCrMo(1280 °C) alloy after potentiodynamic test (SEM).

sintered samples, leading to the possible onset of localized corrosion in the remaining pores. Sintering at 1300 °C led to the material with the highest density and the highest hardness, however, it also led to the beginning loss of dimensional stability, thus, resulting in the loss of the principal advantage of the near net shape technique. The best results were obtained by the treatment at 1280 °C which produced a material with dimensional stability, reasonable density and hardness and with the best repassivation behavior in the Ringer solution.

References

- [1] B.Y. Li, A. Mukasyan, A. Varma, *Materials Research Innovations* 7 (2003) 245.
- [2] P.E. Sinnott-Jones, J.A. Wharton, R.J.K. Wood, *Wear* 259 (2005) 898.
- [3] D. Sun, J.A. Wharton, R.J.K. Wood, L. Ma, W.M. Rainforth, *Tribology International* 42 (2009) 99.
- [4] A. Ouerd, C. Alemany-Dumont, B. Normand, S. Szunerits, *Electrochimica Acta* 53 (2008) 4461.
- [5] F. Contu, B. Elsener, H. Böhni, *Corrosion Science* 47 (2005) 1863.
- [6] M.T. Clarke, P.T.H. Lee, A. Arora, R.N. Villar, *Journal of Bone and Joint Surgery – British Volume* 85-B6 (2003) 913.
- [7] A. Sargeant, T. Goswami, *Materials & Design* 28 (2007) 155.
- [8] N. Rincic, I. Baucic, S. Miko, M. Papic, E. Prohic, *Collegium Aantropologicum* 27 (2003) 99.
- [9] A.W.E. Hodgson, S. Kurz, S. Virtanen, V. Fervel, C.-O.A. Olsson, S. Mischler, *Electrochimica Acta* 49 (2004) 2167.
- [10] M. Metikoš-Hukovic, R. Babic, *Corrosion Science* 49 (2007) 3570.
- [11] H.E. Placko, S.A. Brown, J.H. Payer, *Journal of Biomedical Materials Research* 39 (1998) 292.
- [12] C. Valero Vidal, A. Igual Muñoz, *Electrochimica Acta* 54 (2009) 1798.
- [13] P. Sury, M. Semlitsch, *Journal of Biomedical Materials Research* 12 (1978) 723.
- [14] T.M. Devine, J. Wulff, *Journal of Biomedical Materials Research* 9 (1975) 151.
- [15] F.G. Hodge, T.S. Lee, *Effects of processing on performance of cast prosthesis alloys, Corrosion-NACE* 31 (3) (1975) 111–112.
- [16] S.H. Lee, E. Takahashi, N. Nomura, A. Chiba, *Materials Transactions* 47 (2006) 287.
- [17] C. Montero-Ocampo, A.S. Rodriguez, *Journal of Biomedical Materials Research* 29 (1995) 441.
- [18] C. Song, H. Park, H. Seong, H.F. Lopez, *Metallurgical and Materials Transactions A—Physical Metallurgy and Materials Science* 37A (2006) 3197.
- [19] C.B. Song, H.B. Park, H.G. Seong, H.F. Lopez, *Acta Biomaterialia* 2 (2006) 685.
- [20] Z. Oksiuta, J.R. Dabrowski, W. Ratuszek, *Archives of Metallurgy and Materials* 49 (2004) 949–960.
- [21] Y. Sato, N. Nomura, S. Fujinuma, A. Chiba, *Journal of the Japan Institute of Metals* 72 (2008) 532.
- [22] M. Dourandish, D. Godlinski, A. Simchi, V. Firouzidor, *Materials Science and Engineering A – Structural Materials Properties, Microstructure and Processing* 472 (2008) 338.
- [23] Z. Oksiuta, J.R. Dabrowski, *Powder Metallurgy* 45 (2002) 63.
- [24] F.S. Georgette, in: J.E. Lemons (Ed.), *Effect of hot isostatic pressing on the mechanical and corrosion properties of a cast, porous-coated Co–Cr–Mo alloy, Quantitative Characterization and Performance of Porous Implants for Hard Tissue Applications*, ASTM International, 1987.
- [25] M. Gradzka-Dahlke, J.R. Dabrowski, B. Dabrowski, *Journal of Materials Processing Technology* 204 (2008) 199.
- [26] R. Tandon, in: J.A. Disegi, R.L. Kennedy, R. Pilliar (Eds.), *Net-shaping of Co–Cr–Mo (F-75) via metal injection molding, Cobalt Base Alloys for Biomedical Applications*, ASTM International, 1999.
- [27] ASTM F75-98 Standard specification for cobalt-28 chromium-6 molybdenum alloy castings and casting alloy for surgical implants (UNS R30075).
- [28] D.J. Levine, in: J.E. Lemons (Ed.), *Metallurgical relationship of porous-coated ASTM F75 alloys, Quantitative Characterization and Performance of Porous Implants for Hard Tissue Applications*, ASTM International, 1987.
- [29] A. Kocijan, I. Milošev, D.K. Merl, B. Pihlar, *Journal of Applied Electrochemistry* 34 (2004) 517.
- [30] J.J. Jacobs, R.M. Latanision, R.M. Rose, S.J. Veeck, *Journal of Orthopaedic Research* 8 (1990) 874.
- [31] J.P. Simpson, P.A. Brook, *Journal of Applied Electrochemistry* 4 (1974) 163.
- [32] J. Horvath, H. Uhlig, *J. Electrochem. Soc.* 115 (1968) 791.